Int. J. Electrochem. Sci., 8 **(2013)** 1839 - 1848

International Journal of
ELECTROCHEMICAL
SCIENCE
www.electrochemsci.org

Synthesis, Characterization and Electrochemical Properties of Board-like Al-substituted Alpha Nickel Hydroxides

Hong-Ying Wu[1,*], *Yu-Long Xie*[2], *Zhong-Ai Hu*[1]

[1] College of Chemistry and Chemical Engineering, Northwest Normal University, Lanzhou 730070, PR China
[2] Qinhai University for Nationalities, College of Chemistry and Life Science
[*]E-mail: hongying8860@163.com

Received: 29 November 2012 / *Accepted:* 25 December 2012 / *Published:* 1 February 2013

A board-like Al-substituted α-$Ni(OH)_2$ has been synthesized via a optimizing chemical precipitation method, in which polyethylene glycol is used as the structure-directing reagent. Structural and morphological characterizations of these nanomaterials are performed using powder X-ray diffraction (XRD) and field emission scanning electron microscopy (FESEM). The component and thermal stability of the sample are respectively measured by FT–IR and thermogravimetry (TG). Its electrochemical properties are evaluated by cyclic voltammetry (CV) and galvanostatic charge-discharge technique in 6 M KOH aqueous electrolyte. The results show that the maximum capacity of 331 mAh g^{-1} for 10 mol% Al-substituted α-$Ni(OH)_2$ is obtained at 0.2 C rate. Furthermore, the electrodes have very high discharge rates being able to maintain 93% and 85% of the nominal capacity at the discharge rates of 1.0 and 2.0 C, respectively.

Keywords: Al-substituted α-$Ni(OH)_2$; Precipitation; Electrochemical properties; Nanomaterials; Rechargeable batteries

1. INTRODUCTION

Alkaline rechargeable batteries such as Ni–metal hydride (Ni–MH), nickel–cadmium (Ni–Cd) and nickel–iron (Ni–Fe) are widely applied to today's market covering domains ranging from power tools to portable electronics and electric vehicle [1]. Nickel/metal hydride (Ni/MH) batteries are considered to be one of the most promising choices for electric vehicle (EV) and hydride electric vehicle (HEV) applications due to high power and low cost [2,3]. Nickel hydroxide is an importantly functional material with various applications. It has long been known that nickel hydroxide has a hexagonal layered structure with two polymorphs, α and *β* [4]. Among these phases of nickel hydroxide, *β*-phase is the classical material used in rechargeable batteries. This volumetric capacity has

also been significantly improved upon by the development of spherical $Ni(OH)_2$ grades with high tap densities. However, the long time stability and reversibility in an alkaline electrolyte is still a cause of concern, especially in sealed cells where the swelling of the nickel electrode after repeated overcharge dries out the already very limited amount of electrolyte [5]. Furthermore, the theoretical bulk density is 2.82 g cm^{-3} for the α-phase and 3.97 g cm^{-3} for the *β*-phase, respectively [6]. The *β*-$Ni(OH)_2$ is usually oxidized to *β*-NiOOH in a charge process and has a maximum theoretical specific capacity of 289 mAh g^{-1}. Because α-$Ni(OH)_2$ can be oxidized to *γ*-NiOOH and the average oxidation state of nickel in *γ*-NiOOH is 3.5 or higher, the α-$Ni(OH)_2$ has a superior theoretical specific capacity reaching up to 482 mAh g^{-1} [7–9]. If the theoretical capacity of the α-phase could be more fully utilized, it would compensate for the lower tap density. However, the pure α-$Ni(OH)_2$ is very unstable in water and alkali and quickly transforms to the *β*-phase.

In recent years, a stable α-phase nickel hydroxide as an electrode material has attracted much attention [10–12] since it has not only a higher electrochemical capacity per weight, but also a negligible change of electrode volume when charge–discharge cycling between the α- and γ-phase. The small volume change is connected to a low absorption of water molecules during cycling that facilitates cell design and improves the cycling stability [5]. In order to prepare a stable α-$Ni(OH)_2$, many studies have been carried out through partial substitution of nickel ion in the nickel hydroxide lattice by other metal ions such as Al [13–15], Co [16,17], Fe [18], Mn [19] and Zn [20,21]. Among these metal elements, Al is the most attractive because Al-substituted α-$Ni(OH)_2$ has relatively better electrochemical performance. For further battery applications, single-phase nickel hydroxide products with good crystallinity, homogeneity, uniform morphology with submicrometer particle size distribution, and high surface area are necessary. It has been reported that nickel hydroxide with a smaller crystalline size shows better charge–discharge cyclic characteristics and a higher proton diffusion coefficient [1,22].

In the present work, we report the synthesis, characterization, and electrochemistry properties of board-like nanostructures of nickel hydroxide. The morphology, size, composition, structure, and crystallinity of the products were examined in detail. Furthermore, its advantages as an active material of the positive electrode in rechargeable batteries were discussed.

2. EXPERIMENTAL

2.1. Materials preparation

Reagents were all of AR grade. Water used in the synthesis and washing was deionized.

The α-phase nickel hydroxide has usually poor stability in a strong basic medium and transforms readily to the *β*-phase after a few electrochemical charge–discharge cycles [23–25]. However, stability of α-phase nickel hydroxide can be achieved after a 20 mol% substitution of nickel by other metal ions [26–29], in particular with trivalent ions such as Al^{3+} [30–33]. On the other hand, substitution in the α-phase nickel hydroxide should be as low as possible in order to retain a high capacity and energy density. Hence, the stable α-phase nickel hydroxide having the Al content of 10

%, 20 %, and 30% (in mole ratio) was prepared in this study as follows: the molar ratio of the $Ni(NO_3)_2 \cdot 6H_2O$:$Al(NO_3)_3 \cdot 9H_2O$ were 9:1, 8:2, and 7:3, respectively; these were dissolved in deionized water to give solutions (50 mL) with a $\{[Ni^{2+}] + [Al^{3+}]\}$ concentration of 0.2 mol/L, and then 10g polyethylene glycol was added to the solution under vigorous stirring for 1 h. The aqueous solution of $NH_3 \cdot H_2O$ (25%–28%) was dropwise added into the above solution with continuous stirring until the pH of the solution reached 9. After aging for 12 h, the resulting product was separated by suction filtration and rinsed with distilled water and ethanol several times, and then dried at 60 °C for 12 h under vacuum.

2.2. Characterization

The morphology of nickel hydroxide electrode was investigated by field emission scanning electron microscopy (FESEM) (JSM-6701F, Japan). Their structure and components were measured by X-ray diffraction (D/Max-2400) with Cu Kα radiation (λ = 1.5418 Å) operating at 40 kV, 60mA and a Nicolet Nexus 670 FT–IR instrument, respectively. Thermal analyses, including thermogravimetry analysis were carried out using a Perkin-Elmer TG/DTA–6300 instrument evolved during sample heating. A heating rate of 10 °C min^{-1} in nitrogen with a flow rate of 20 mL min^{-1} was used.

2.3. Electrode preparation and electrochemical characterization

Electrodes for electrochemical capacitors were prepared by mixing the active materials with 10 wt.% acetylene black, 10 wt.% conducting graphite and 5 wt.% polytetrafluoroethylene (PTFE) of the total electrode mass. A small amount of ethanol was added to this composite to make a more homogenous mixture, which was pressed on nickel foam sheet. Electrochemical measures on the Al-substituted α-$Ni(OH)_2$ were carried out on a CHI660B electrochemical working station (CH Instrument). A typical three-electrode cell was employed. The electrolyte was 6 M KOH solution. The prepared electrode with a geometric area of 1 cm^2 was used as the working electrode. A platinum foil served as the counter electrode and Hg/HgO as the reference electrode. Galvanostatic charge–discharge studies were conducted using a LAND model CT2001A battery-test system. The working electrode was galvanostatically charged at 0.2 C rate for 6 h, rested for 5 min, and then was discharged to 0.1V versus Hg/HgO.

3. RESULTS AND DISCUSSION

3.1. Material characterization

Fig. 1 presents XRD patterns of the α-$Ni(OH)_2$ samples prepared in this project. The patterns in Fig. 2 comprise four broad peaks appearing at 2θ values of 11.1° (7.98Å), 22.4° (3.97Å), 34.5° (2.60Å) and 60.7° (1.52Å), which are similar to the standard XRD pattern of α-$4Ni(OH)_2 \cdot 3H_2O$

(JCPDS 38-0715). It is well known that α-$Ni(OH)_2$ and *β*-$Ni(OH)_2$ crystallize as a hexagonal system with the brucite-type structure and with $Ni(OH)_2$ layers stacked along the *C*-axis. Each $Ni(OH)_2$ layer consists of a hexagonal planar arrangement of octahedrally oxygen coordinated Ni(II) ions. The main difference between α-$Ni(OH)_2$ and *β*-$Ni(OH)_2$ resides in the stacking of the layers along the *C*-axis. *β*-$Ni(OH)_2$ layers are perfectly stacked along the *C*-axis with an interlamellar distance of 4.6 Å, but α-$Ni(OH)_2$ layers are randomly oriented and separated by intercalated water molecules bonded to the hydroxyl groups by hydrogen bonds [34].

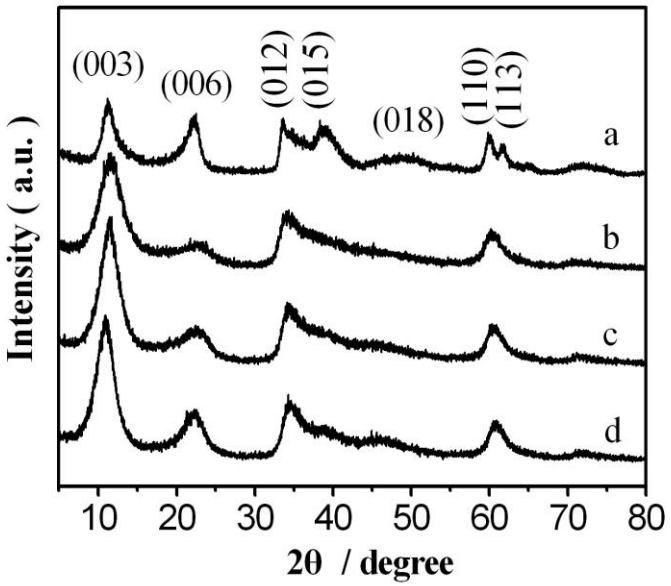

Figure 1. XRD patterns of the samples: (a) 10 mol% Al-substituted α-$Ni(OH)_2$ after ageing for 20 days in 6 M KOH; fresh (b) 10 mol%, (c) 20 mol % and (d) 30 mol% Al-substituted α-$Ni(OH)_2$

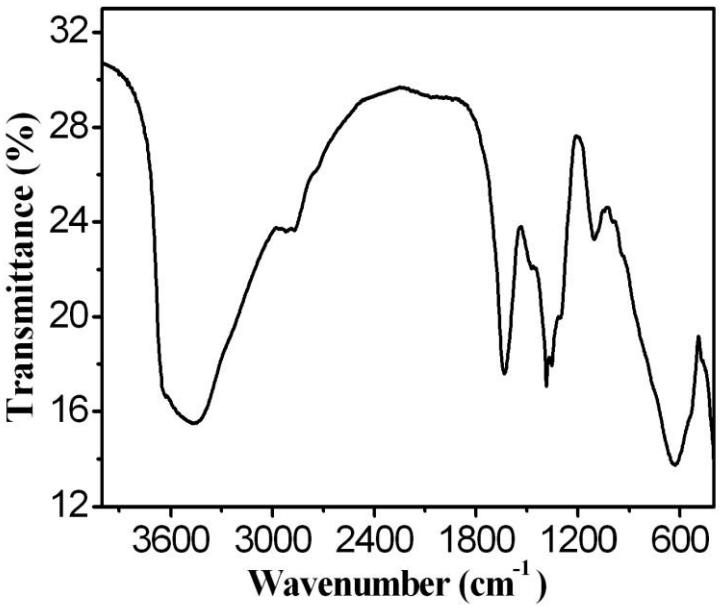

Figure 2. FTIR spectra of the 10 mol% Al-substituted α-$Ni(OH)_2$.

The interlamellar distance for the α-$Ni(OH)_2$ is about 8 Å. The XRD pattern of aluminum stabilized α-$Ni(OH)_2$ is the same as that of unsubstituted α-$Ni(OH)_2$ as reported in literature [35]. The XRD pattern of stabilized α-$Ni(OH)_2$ in Fig. 1(curve b, c, and d) displays a low angle reflection close to 8 Å, followed by another at around 4 Å. The results are in agreement with values found by Kamatt et al. [36] and Indira et al. [37] for the layered double hydroxides (LDHs) of nickel with aluminum. All the peaks of the powders synthesized in this study can be indexed to those of α-$Ni(OH)_2$ with a slight shift in the (0 0 3) and (0 0 6) peak positions. These shifts are attributable to the extent and type of the intercalated anions (CO_3^{2-}, NO_3^- etc.) in the $Ni(OH)_2$ lattice. No peaks from β-$Ni(OH)_2$ were observed in any pattern, indicating that the precipitated powders are pure α-phase, at least at the XRD detection level.

In order to test the stability of the samples in the concentrated alkaline medium, the 10 mol% Al-substituted nickel hydroxides were aged in 6 M KOH for 20 days. The XRD patterns is shown in Fig. 1(curve a), the sample retain the α-phase and the peaks become sharper and stronger after ageing for 20 days, which indicates that their crystallinity has increased. The ageing treatment induces a loss of turbostatic characteristics and a recrystallization process occurs. This indicates that the addition of Al leads to higher crystallinity and increases the structural stability in alkaline medium.

To further support the XRD study, the FT-IR spectrum of the sample was presented in Fig. 2. A trace amount of interlayer CO_3^{2-} anions may result from the slight dissolution of CO_2 from air. The incorporation of water molecules and CO_3^{2-} ions is evidenced by the FT-IR spectrum as depicted in Fig. 2. The large band centered at 3500 cm^{-1} is assigned to the O–H stretching modes of interlayer water molecules and of H-bound OH group, and the peak at 1640 cm^{-1} is due to the bending mode of water molecules [38–40]. The intense and sharp band at 1383 cm^{-1} is characteristic of interlayer NO_3^-. Other absorptions below 1000 cm^{-1} are associated with Ni–O stretching and Ni–OH bending vibrations.

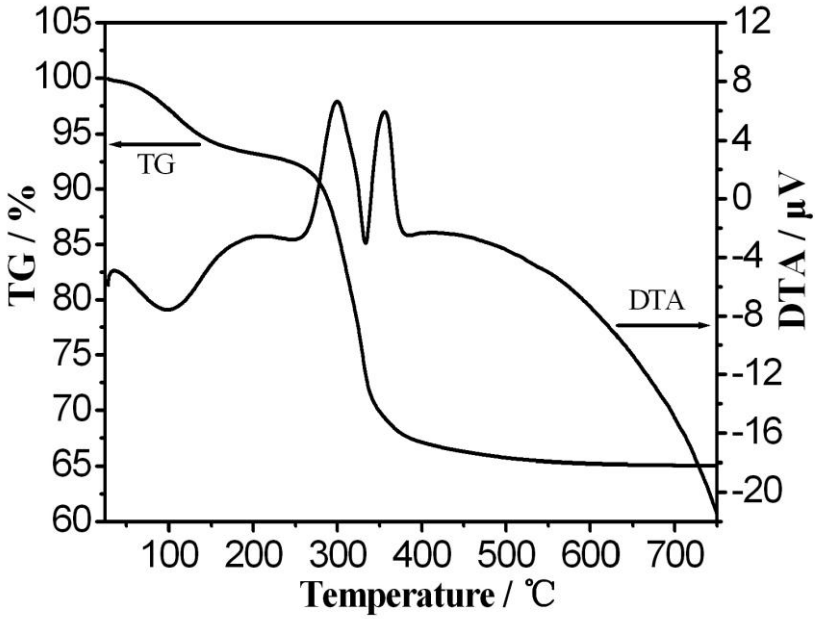

Figure 3. TG/DTA analysis of nickel hydroxide.

Figure 3 shows the TG curve of the α-$Ni(OH)_2$ sample in the temperature range of 25–750 ℃. The α-phase underwent weight loss of 38.8 % in four steps indicated by the zones Ⅰ, Ⅱ, Ⅲ, and Ⅳ on the graph. The weight loss below 50 ℃ (domain Ⅰ) is ascribed to the removal of the absorbed water. The weight loss (11.5%) between 50 and 207 ℃ (domain Ⅱ) is assigned to the evaporation of the intercalated water molecules. Domain Ⅲ ranging from 207 to 340 ℃ is associated with the loss of water produced by dehydroxylation of the hydroxide layers combined with the partial loss of the anionic species (NO_3^- and CO_3^{2-}). Finally, the fourth domain (domain Ⅳ) ending at about 600 ℃ can be attributed to the loss of NO_3^- ions.

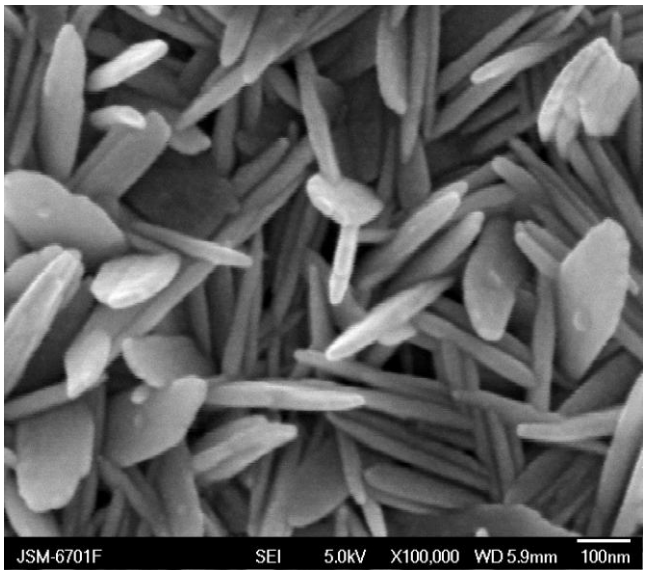

Figure 4. FESEM images of the 10 mol% Al-substituted α-$Ni(OH)_2$.

The morphology of the as-prepared α-$Ni(OH)_2$ was observed by FESEM. Typical FESEM image shown in Fig. 4 reveal that the Al-substituted α-$Ni(OH)_2$ synthesized in the present work display an almost perfect board-like morphology and that these platelets are rather thin and uniform. The platelets are estimated to be 20~30 nm in the length and about 10 nm in the thickness. It has been identified that the size, morphology and structure of the materials have a crucial effect on its electrochemical behavior. It is evident that the nanostructured board-like Al-substituted α-$Ni(OH)_2$ facilitates geometrically to construct a highly micro-porous structure, which counteracts agglomeration of the active materials and increases the liquid-solid interfacial area. Also, the presence of loose structure gives much more accessibilities for OH^- insertion and extraction or results in a material having high density of active sites for promoting fluid/solid reactions [41].

3.2. Electrochemical characterization

Cyclic voltammograms for electrodes with different aluminium contents are given in Fig. 5. Only one anodic oxidation peak for the electrode with 10 mol% Al (at about 519 mV) was recorded prior to oxygen evolution. Correspondingly, only one oxyhydroxide reduction peak at about 318 mV

was observed on the reverse sweep. Similar voltammograms were observed for an electrode with a higher aluminium content (20 mol% and 30 mol% Al), but the anodic peak corresponding to nickel hydroxide oxidation and the cathodic peak corresponding to nickel oxyhydroxide reduction shift to more positive and negative potentials respectively, compared with those of the electrode with 10 mol% Al.

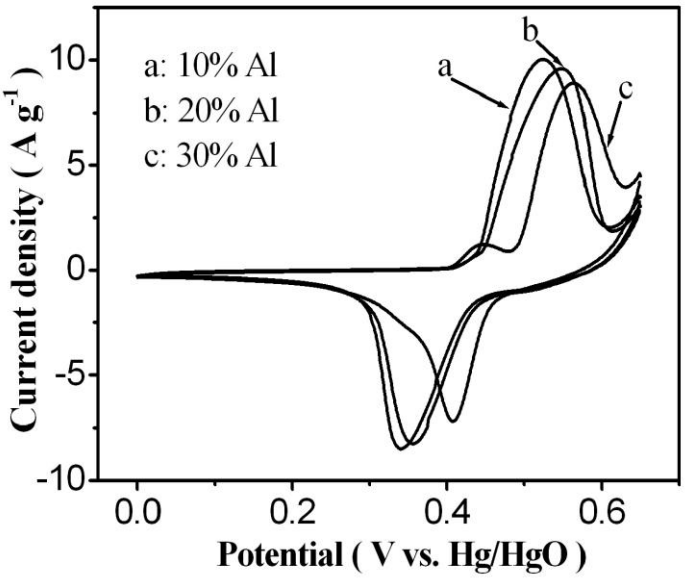

Figure 5. Cyclic voltammograms curves of the 10, 20 and 30 mol% Al-substituted α-$Ni(OH)_2$ at scan rate of 1 mV s^{-1} within a potential window of 0 to 0.65 V.

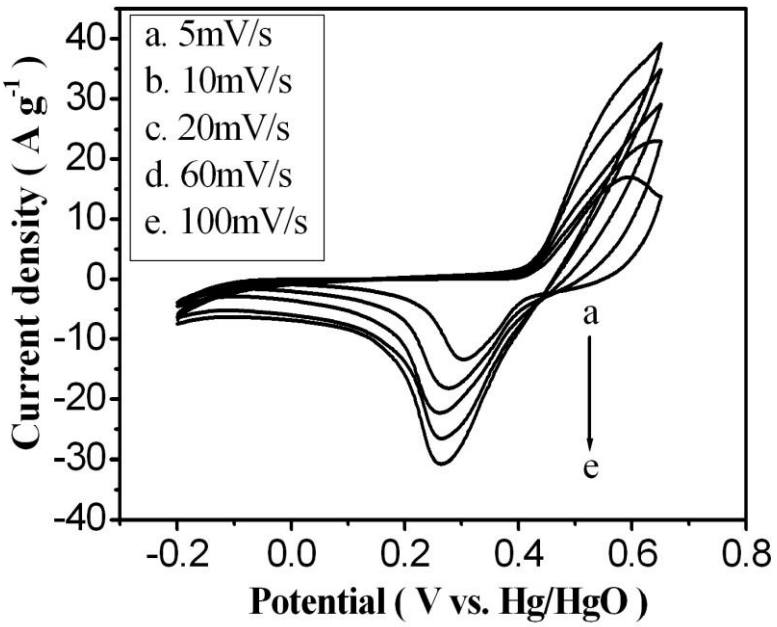

Figure 6. Cyclic voltammograms of 10 mol% Al-substituted α-$Ni(OH)_2$ electrode at different scan rates.

Typical cyclic voltammograms for10 mol% Al-substituted nickel hydroxide at various scan rates are shown in Fig. 6. As the scan rate increases, the anodic peak potential shift in a more positive direction, and the cathodic peak potential shift in a more negative direction. The current of oxidation and reduction peaks of the $Ni(OH)_2$ electrode with 10 mol% (wt.%) Al increases gradually with the scan rate increases.

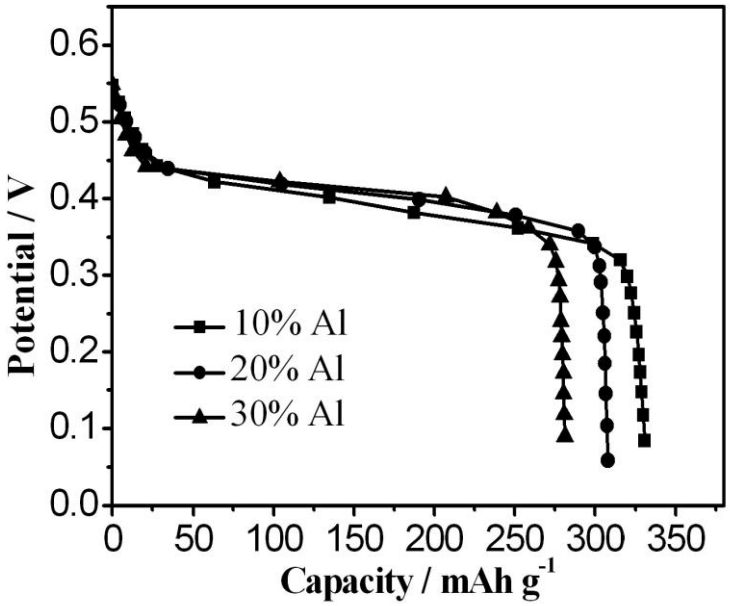

Figure 7. The discharge curves of the 10, 20 and 30 mol% Al-substituted α-$Ni(OH)_2$ at 0.2C rate.

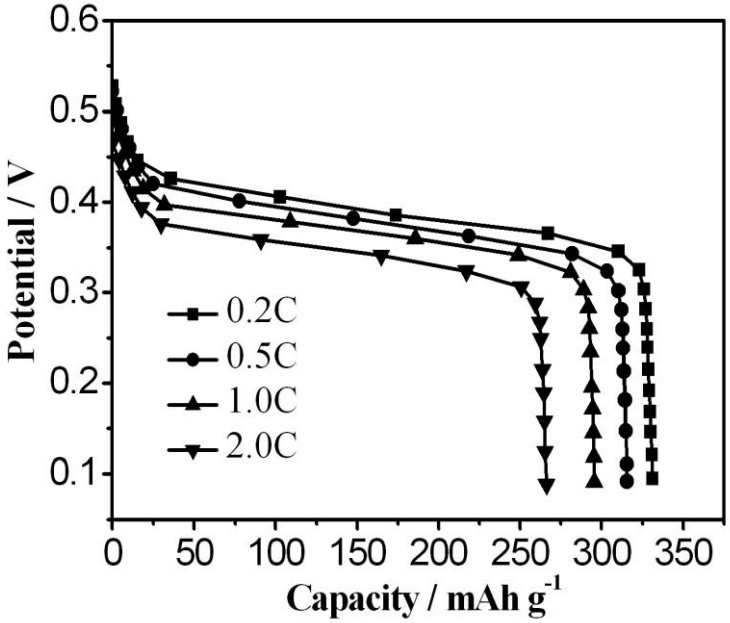

Figure 8. The discharge curves of 10 mol% Al-substituted α-$Ni(OH)_2$ samples at 0.2 C, 0.5 C, 1.0 C, and 2.0 C rate.

Fig. 7 shows the discharge curves of the different aluminium contents electrodes at the 0.2 C rate. It can be seen that all the discharge curves are very flat and the discharge potential increases with increase in Al content at 0.2 C. The highest discharge capacity of 331 mAh g^{-1} is obtained at 0.2 C rate in the case of 10 mol% Al-substituted α-$Ni(OH)_2$. The discharge capacity is slightly decreased with increasing Al content at the 0.2 C rate. The other two samples had capacities of 308 mAh g^{-1} and 281 mAh g^{-1}. The highest discharge capacity obtained in this work is very close to that of 20.4% Al substituted-$Ni(OH)_2$ hollow spheres [42] and nickel–aluminum layered double hydroxide/carbon composite with 17.8 Al% [43].

Fig. 8 shows the relationship between the discharge capacity and discharge rates from 0.2 to 2.0 C. The α-type nickel hydroxide can sustain very high discharge rates, being able to maintain 93% and 85% of the nominal capacity at the discharge rates of 1.0 and 2.0 C, respectively. This is significantly better than the α-type nickel electrodes, as seen in Fig. 8. The superior rate capability of the α-phase nickel hydroxide is probably related to its larger interlayer spacing about 7.98 Å, allowing for a better proton mobility compared with the *β*-phase nickel hydroxide having an interlayer distance of 4.6 Å [44, 45].

4. CONCLUSIONS

An Al-substituted α-$Ni(OH)_2$ were synthesized via a optimizing chemical precipitation method. The experimental results of XRD indicate that the samples are typical α-phase. The SEM images exhibit that the Al-substituted α-$Ni(OH)_2$ prepared in the present work display board-like morphology. The electrodes show the maximum capacity of 331 mAh g^{-1} for 10 mol% Al-substituted α-$Ni(OH)_2$ at 0.2 C rate, and have very high discharge rates being able to maintain 93% and 85% of the nominal capacity at the discharge rates of 1.0 and 2.0 C, respectively. Because of their unique structures and properties, the board-like of nickel hydroxide may give a new perspective for applications in the areas of rechargeable batteries.

ACKNOWLEDGEMENTS
The authors gratefully acknowledge the financial support offered by the National Natural Science Foundation of China (20963009, 21163017).

References

1. X. Liu, L. Yu, *J Power Sources* 128 (2004) 326.
2. D. Ohms, M. Kohlhase, G. Benczúr-Űrmőssy, G. Schädlich, *J Power Sources* 105 (2002) 127.
3. W.K. Zhang, X.H. Xia, H. Huang, Y.P. Gan, J.B. Wu, J.P. Tu, *J Power Sources* 184 (2008) 646.
4. P. Oliva, J. Leonardi, J.F. Laurent, C. Delmas, J.J. Braconnier, M. Figlarz, F. Fievet, A. De Guibert, *J. Power Sources* 8 (1982) 229.
5. W.K. Hu, X.P. Gao, D. Noréus, T. Burchardt, N.K. Nakstad, *J Power Sources* 160 (2006) 704.
6. M. Oshitani, T. Takayama, K. Takashima, S. Tsuji, *J. Appl. Electrochem*. 16 (1986) 403.
7. C. Faure, C. Delmas, M. Fouassier, *J. Power Sources* 35 (1991) 279.
8. D.A. Corrigan, S.L. Knight, *J. Electrochem. Soc.* 136 (1989) 613.

9. D. Yang, R. Wang, M. He, J. Zhang, Z. Liu, *J. Phys. Chem*. B 109 (2005) 7654.
10. C.Y. Wang, S. Zhong, D.H. Bradhurst, H.K. Liu, S.X. Dou, *J. Alloys. Compd*. 802 (2002) 330.
11. R.S. Jayashree, P.V. Kamath, *J Power Sources* 107 (2002) 120.
12. W.K. Hu, D. Noréus, *Chem Mater* 15 (2003) 974.
13. Y.L. Zhao, J.M. Wang, H. Chen, T. Pan, J.Q. Zhang, C.N. Cao, *Electrochim. Acta* 50 (2004) 91.
14. A. Sugimoto, S. Ishida, K. Hanawa, *J. Electrochem. Soc*. 146 (1999) 1251.
15. Y.J. Leng, B. Liu, F.J. Wang, Y. Xiao, Z.F. Ma, Chin. *J. Power Sources* 24 (2000) 326.
16. C. Faure, C. Delmas, P. Willmann, *J. Power Sources* 36 (1991) 497.
17. J.Y. Xie, Q.S. Zhang, J.F. Liu, P.F. Shi, Chin. *J. Power Sources* 23 (1999) 238.
18. L. Demourgues-Guerlon, C. Delmas, *J. Power Sources* 45 (1993) 281.
19. L. Demourgues-Guerlou, L. Fournes, C. Delmas, *J. Electrochem. Soc*. 143 (1996) 561.
20. M. Dixit, P.V. Kamath, J. Gopalakrishnan, *J. Electrochem. Soc*. 146 (1999) 79.
21. C. Tessier, L. Guerlou-Demourgues, C. Faure, M. Basterreix, G. Nabias, C. Delmas, *Solid State Ion.* 133 (2000) 11.
22. K. Watannabe, T. Kikuoka, *J. Appl. Electrochem*. 25 (1995) 219.
23. A. Delahaye-Vidal, B. Beaudoin, N. Sac-Epee, K. Tekaia-Elhsissen, A. Audemer, M. Figlarz, *Solid State Ionics* 84 (1996) 239.
24. H. Bode, K. Dehmelt, J. Witte, *Electrochim. Acta* 11 (1966) 1079.
25. R.S. McEwen, *J. Phys. Chem*. 75 (1971) 1782.
26. L. Demourgues-Guerlou, C. Delmas, *J. Electrochem. Soc*. 141 (1994) 713.
27. R.S. Jayashree, P.V. Kamath, *J. Power Sources* 107 (2002) 120.
28. B. Liu, X.Y. Wang, H.T. Yuan, Y.S. Zhang, D.Y. Song, Z.X. Zhou, *J. Appl. Electrochem*. 29 (1999) 853.
29. L. Demourgues-Guerlou, C. Delmas, J. Power Sources 52 (1994) 269.
30. K.T. Ehlsissen, A. Delahaye-Vidal, P. Genin, M. Figlarz, P. Willmann *J. Mater. Chem*. 3 (1993) 883.
31. A. Sugimoto, S. Ishida, K. Hanawa, *J. Electrochem. Soc*. 146 (1999) 1251.
32. J. Dai, S.F.Y. Li, T.D. Xiao, D.M. Wang, D.E. Reisner, *J, Power Sources* 89 (2000) 40.
33. G.A. Caravaggio, C. Detellier, Z. Wronski, *J. Mater. Chem*. 11 (2001) 912.
34. L. Bing, Y. Huatang, Z. Yunshi, Z. Zuoxiang, S. Deying, *J. Power Sources* 79 (1999) 277.
35. M.C. Bernard, P. Bernard, M. Keddam, S. Senyarich, H. Takenouti, *Electrochim. Acta* 41 (1996) 91.
36. P.V. Kamath, M. Dixit, L. Indira, A.K. Shukla, V.G. Kumar, N. Munichandraiah, *J. Electrochem. Soc*. 141 (1994) 2956.
37. L. Indira, M. Dixit, P.V. Kamath, *J. Power Sources* 52 (1994) 93.
38. P. Jeevanandam, Yu. Koltypin, Y. Mastai, *J. Mater. Chem*. 10 (2000) 511.
39. Z. P. Xu, H.C. Zeng, *Chem. Mater*. 11 (1999) 67.
40. Y. Zhu, h. Li, Y. Koltypin, A. Gedanken, *J. Mater. Chem*. 12 (2002) 729.
41. J.M. Luo, B. Gao, X.G. Zhang, *Materials Research Bulletin*. 43 (2008) 1119.
42. Y. Li, W. Li, S. Chou, J. Chen, *J. Alloys Compd*. 456 (2008) 339.
43. A.B. Béléké, M. Mizuhata, *Journal of Power Sources* 195 (2010) 7669.
44. W.K. Hu, D. Noréus, *Chem. Mater*. 15 (2003) 974.
45. L.J. Yang, X.P. Gao, Q.D. Wu, H.Y. Zhu, G.L. Pan, *J. Phys. Chem. C* 111 (2007) 4614.